

Free Energy Approaches for Modeling Atomic Force Microscopy in Liquids

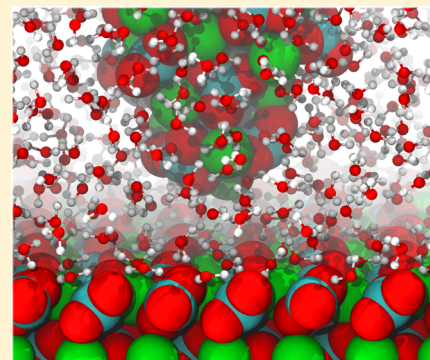
Bernhard Reischl,^{*,†,‡} Matthew Watkins,[§] and Adam S. Foster[‡]

[†]Tampere University of Technology, Department of Physics, P.O. Box 692, FI-33101 Tampere, Finland

[‡]COMP Centre of Excellence, Aalto University School of Science, Department of Applied Physics, P.O. Box 11100, FI-00076 Aalto, Finland

[§]London Centre for Nanotechnology and Department of Physics and Astronomy, University College London, Gower Street, London, WC1E 6BT, United Kingdom

ABSTRACT: High resolution atomic force microscopy (AFM) in liquids offers atomic scale insight into the structure at water/solid interfaces and is perhaps the only tool capable of resolving the nature of formed hydration layers. However, convolution between the imaging signal and the tip/surface interactions and hydration layers means that interpretation is far from straightforward. Modeling the complex imaging mechanism of atomic force microscopy in liquids requires calculation of the free energy profile as a function of the distance between AFM tip and surface. Its derivative is the best approximation for the force acting on the AFM tip, including entropic contributions from interactions with water molecules in hydration layers over the surface and around the tip apex. In order to establish a reliable approach for these simulations, we compare two methods of calculating free energy profiles from atomistic molecular dynamics simulations, umbrella sampling and free energy perturbation, on two model surfaces, calcium fluoride and calcium carbonate. Our results demonstrate that both methods effectively provide equivalent free energy profiles but offer different possibilities in terms of efficiency, constraints, and analysis of the free energy components.



1. INTRODUCTION

Following the development of atomic force microscopy (AFM) as a powerful tool for studies of surfaces in general, the scope of its application has widened dramatically, with a particularly important impact on studies in liquid environments.¹ For example, AFM has been a breakthrough experimental technique in protein folding,^{2,3} where it has been possible to make a direct link between the measured force variations and free energy change of the unfolding transition—providing unprecedented insight into the folding mechanism itself. In terms of local studies, imaging in liquids now challenges the high resolutions that have been achieved under vacuum conditions,⁴ offering the potential to even map individual water molecules in hydration structures. In general, atomic resolution is achieved by operating the AFM in frequency modulation (FM) or noncontact (nc-AFM) mode;⁵ the cantilever oscillation is driven at its instantaneous eigenfrequency, with constant amplitude, and the site-dependent change in cantilever frequency (frequency shift) Δf is measured as the surface is scanned. Measurements of the frequency shift as a function of tip position allow the buildup of 2D topological images of the surface, or by turning off the feedback loops that control the tip location and instead following prescribed trajectories, 3D maps of the frequency shift above a surface can be built up. The development of low amplitude AFM techniques has proved to be a breakthrough in difficult environments, with particular success demonstrated in high resolution imaging in liquids.^{6–9}

Recent developments in speed and control mean it is possible to even perform 3D imaging in water, and this was applied to obtain unprecedented resolution of the structure of water layers on mica¹⁰ and on molecular layers of different hydrophobicity.¹¹ The frequency vs distance curves measured in the 3D mode (so-called “force spectroscopy”) are not monotonic but exhibit features that can be ascribed to water structuring above the surface. There are now well established formulas in the literature allowing the frequency shift to be converting into a quantitative force measurement,¹² which can be directly compared to force curves derived from the free energy of the system. This provides an opportunity to use AFM in liquids as a benchmark to demonstrate the accuracy of free energy approaches. In much the same way, a fascinating variant on the AFM has been used to probe nanoscale van der Waals interactions without the limitations of averaging over large planar surface areas.¹³ In preparation for this, we first need to establish an appropriate free energy simulation methodology for modeling AFM in liquids.

In order to provide a full atomistic understanding of the forces being measured in AFM experiments in liquids, it is important that we can demonstrate that simulations can be performed reproducibly, without bias from technical simulation parameters, with correct boundary conditions, and remain

Received: September 26, 2012

Published: November 30, 2012

computationally feasible. Calculating free energy curves to compare to experimentally recovered AFM data places a burden on the computational techniques chosen: we need to calculate curves over a wide range of tip and sample separations at high resolution and with high accuracy; the magnitude of experimental forces is such that we need to converge statistical errors below ~ 5 kJ/mol over multiple (~ 10 s to even 100s) simulations. Due to the experimental method where the tip is oscillated and can sample large areas of the free energy surface, we cannot restrict our attention to particular regions of interest around free energy minima. Furthermore, calculations must be carried out at multiple lateral locations above the surface in order to reveal the ability of the microscope tip to achieve atomic resolution. Compared to other types of systems, such as studies of interactions between nanoparticles or proteins with biological membranes, hydrophobic interactions, or low-resolution mode AFM, where similar free energy calculation techniques have been more frequently applied,^{14–19} our simulations require subtly different boundary conditions: the tip must remain fixed with respect to rotation about its vertical axis to reflect the experimental geometry, and as the tip is sharp to avoid averaging over larger areas, care must be taken to obtain statistically converged values.

Compared to AFM experiments in a vacuum, there is strong viscous damping in the liquid. To limit oscillator noise, stiff cantilevers (spring constant $k \sim 30\text{--}50$ N/m) are used, and the oscillation amplitudes Δz are very small, between 0.1 and 0.5 nm, which is on the same order as the diameter of a single water molecule. Typical cantilever oscillation frequencies are on the order of 150 kHz. This means that any dynamics with higher frequency will be averaged over, and we can consider the system to be in equilibrium during an oscillation cycle. This is the justification for calculating free energy profiles as a function of the tip–surface distance, for different lateral positions of the tip, and taking the derivative as an approximation for the short-range force measured by the AFM tip. In principle, it would be possible to go further and follow the system from equilibrium to nonequilibrium dynamics, which would move toward nanotribological applications,²⁰ but here we restrict ourselves to the equilibrium case. Hence, the method we present cannot be used to study site-specific energy dissipation often observed in actual AFM experiments, which is the result of different force–distance curves being followed during approach and retraction of the tip.^{21–23}

Recent atomically resolved FM-AFM images of the calcite (10 $\bar{1}$ 4) surface in water,⁸ at some tip–surface distances, resemble those obtained in UHV.²⁴ However, in liquid the contrast mechanism is much more complicated, showing a much richer variety of contrast patterns as the tip approaches the surfaces and samples different interaction regimes. Since the experimental data for imaging calcite both in a vacuum and water is readily available, we choose it as one of our example systems. In order to generalize our methodology and conclusions we also study another ionic crystal surface, calcium fluoride (111). Figure 1 illustrates the different surface geometries of calcite (10 $\bar{1}$ 4) and fluorite (111). The fluorite surface has been studied extensively under high-resolution vacuum conditions in combined experiments and simulations,²⁵ and the interactions in liquids have been considered theoretically using a free energy perturbation approach.^{26,27} In combination, these two materials are representative of a wide variety of characteristic surfaces—fluorite is a rigid ionic system, while the calcite crystal introduces much more molecular

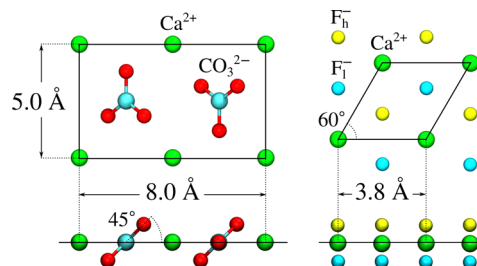


Figure 1. The unit cells of the calcite (10 $\bar{1}$ 4) (left) and fluorite (111) surfaces (right), seen in top and side views. The rectangular calcite surface unit cell contains two calcium and carbonate ions, due to the two opposite orientations of carbonate groups. Each carbonate ion has one oxygen atom above, one below, and one in the surface plane. In the rhombic fluorite surface unit cell, one fluoride ion is situated above (F_h) and one below (F_l) the surface plane of calcium ions.

flexibility and potential for complex atomic rearrangements. Hence, we feel the study will have general relevance to modeling solid/liquid interfaces in other ionic materials, such as oxides, while also impacting characterization of softer materials like organic crystals or lipid/protein membranes.

The remainder of this article is organized as follows: In section 2 we explain the model system used to simulate AFM in liquids and give a short summary of the two free energy calculation methods used, umbrella sampling and free energy perturbation. In section 3, we present free energy profiles for calcite and fluorite. In sections 4 and 5, we compare the free energy profiles obtained with two different methods and discuss the accuracy of the methods and their robustness with respect to changes in simulation parameters, using fluorite as a benchmark system.

2. METHODS

2.1. Simulating AFM in Liquids. In order to simulate AFM in liquids, several simplifications need to be made, as illustrated in Figure 2a. The changes in the interactions between the AFM tip, surface, and liquid, responsible for high resolution images, depend mostly on atoms in a limited region of space around the apex and surface. We set up a model of the interface as follows: the simulation box contains several layers of the surface material, and the remaining volume is filled with liquid. To obtain a simulation box compatible with periodic boundary conditions, we model the AFM tip with a nanocluster of the material most likely covering the apex region of the tip. To account for the missing macroscopic part of the tip and cantilever, the nanocluster needs to be constrained to avoid translational or rotational motion.

Silicon cantilever tips, typically used for imaging in liquids, are covered in an amorphous silicon dioxide layer. In contact with water, this SiO₂ surface will further react and form silanol groups, Si–OH. In addition, the solution contains ions dissolved from the sample surface, or other buffer ions added to stabilize the system, which might aggregate on the tip surface. Finally, the contrast obtained in frequency shift images—which reflects the differences in site-specific interactions between tip, surface, and liquid—may be enhanced after deliberately (or accidentally) crashing the tip into the surface, which would hint at the tip apex then being covered in surface material. This is known to work under vacuum conditions and can sometimes be achieved in water as well.²⁸ In view of the ambiguities concerning the exact nature of the tip, we model the nanocluster representing the tip apex of the same material

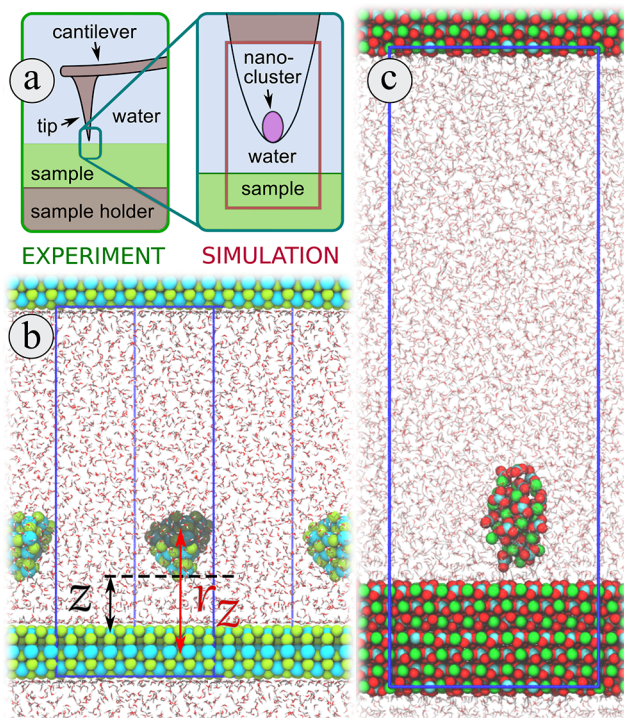


Figure 2. The simulation setup. (a) The apex of the AFM tip is modeled as a nanocluster of the same material as the surface. (b) Snapshot of the fluorite simulation: calcium atoms are colored in cyan and fluorine in green. Water molecules are represented as red and white licorice molecules. Blue lines indicate the borders of the rhombohedral simulation cell. The harmonic umbrella potential acts on the r_z component of the vector between the center of mass of the surface slab and the center of mass of the constrained part of the nanocluster tip, shaded in gray. The “tip–surface distance” z designates the distance between the lowest atom in the tip and the topmost plane of calcium atoms in the surface. (c) Snapshot of the calcite simulation: calcium atoms are colored in green, carbon in cyan, and oxygen in red.

as the surface. This has the benefit of reducing the number of atomic species in the system and the number of force field parameters needed to describe their interactions.

To gather statistically meaningful values of the force on the AFM tip as a function of the tip–surface distance, multiple oscillation cycles of microsecond duration would need to be simulated in steered molecular dynamics. Fortunately, the microsecond time scale of the cantilever oscillation is much slower than the time scale of librational motion or diffusion of water molecules at room temperature. We therefore assume that the system is in, or close to, equilibrium throughout an oscillation cycle. In previous studies of fluorite in water,^{26,27} we established the importance of entropic effects on the force measured by the AFM tip, due to the presence of hydration layers on top of the surface, as shown in Figure 3, hence the need to perform free energy calculations, in an appropriate statistical ensemble. The force on the AFM tip f is then given by the derivative of the free energy, with respect to the tip–surface separation distance z . In the canonical ensemble (constant particle number N , volume V , and temperature T):

$$f_{NVT}(z) = -\frac{\partial F(N, V, T; z)}{\partial z} \quad (1)$$

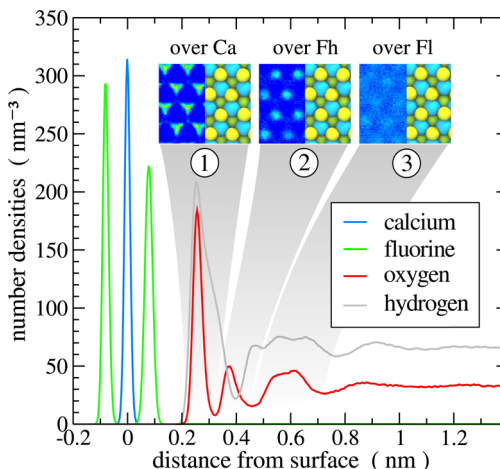


Figure 3. Hydration layer structure over fluorite (111) from simulation. Density profiles along z , perpendicular to the surface, indicate that there are three distinct hydration layers over the surface. Small insets show water molecule oxygen density maps in (x,y) planes within the hydration layers and atomic positions in the surface underneath: water molecules in the first hydration layer are located above the surface calcium atoms (cyan), and second layer water molecules are situated above the protruding fluorine atoms (yellow). Water molecules in the third hydration layer exhibit less order in (x,y), but their density is increased above the subsurface fluorine atoms (green).

with the Helmholtz free energy $F = U - TS$, where U and S denote the internal energy and entropy, respectively. In the isobaric–isothermal ensemble (constant particle number N , pressure p , and temperature T),

$$f_{NpT}(z) = -\frac{\partial G(N, p, T; z)}{\partial z} \quad (2)$$

where $G = U - TS + pV$ denotes the Gibbs free energy, or free enthalpy.

2.2. Umbrella Sampling. Umbrella sampling is a well established method used to compute a free energy profile as a function of a collective variable, also referred to as a potential of mean force (PMF).^{29,30} In our work, the collective variable z corresponds to the r_z component of the distance vector $\mathbf{r} = \{r_x, r_y, r_z\}$ between the centers of mass of the tip and surface, for a given lateral position of the tip. The free energy profile is then given by:

$$F(z) = -k_B T \ln P(z) + \text{const} \quad (3)$$

where k_B denotes Boltzmann’s constant, T the temperature, and $P(z)$ the probability distribution of z measured in the simulation. The accuracy of such a free energy profile is limited by the fact that configurations of the system with a high free energy will be visited rarely (or not at all) during the course of the computer simulation. The error of the sampled distribution $P(z)$ will be large around the corresponding values of the collective variable, resulting in a large error of the computed free energy profile $F(z)$. Therefore, it is advantageous to divide the problem into N independent simulations of systems in which the value of z is constrained to some intermediate value, $z_{\min} < z_0^i < z_{\max}$, by a harmonic umbrella potential, $U_i(z) = k_i(z - z_0^i)^2$, for $i = 1, \dots, N$. In each of these simulations (called umbrella windows), a biased distribution $P_i(z)$ is then sampled with good accuracy, over a range of $\Delta z \approx (k_B T / k_i)^{1/2}$. If there is sufficient overlap between the

distributions in neighboring windows, the global, unbiased, distribution can be reconstructed through histogram reweighting methods, and a continuous profile of $F(z)$ is obtained. Assuming that all degrees of freedom orthogonal to the collective variable have been sampled sufficiently, the free energy calculated in this way is an equilibrium property of the system.

2.3. Free Energy Perturbation. As in our previous publications, we calculated the short-range force exerted on the tip from the derivative of the potential of mean force along the direction of tip approach;^{26,27} this force is equivalent to the force required to hold the constrained ions in place and thus to the force that would be transferred to the AFM cantilever. PMFs were calculated using the free energy perturbation method (FEP) of Zwanzig³¹ by performing simulations with a numerical setup similar to that used in refs 32 and 19. To perform this sampling, part of the tip furthest from the surface and the central layers of the substrate were frozen and not allowed to move during each simulation. Between simulations, the z coordinates of all tip ions were moved toward the surface in small ($0.01\text{--}0.015\text{ nm}$) steps. Freezing the top of the tip ensures that it has no rotational freedom, which reflects the fact that in the real experiment the nanotip is a continuation of a much larger, macroscopic tip. Configurations were sampled every few picoseconds from trajectories of several nanoseconds and saved for further analysis. The sampled configurations from the trajectory were then perturbed by rigidly moving the tip half the distance between successive simulations, along the z axis. Errors at each tip height could be estimated from block averaging the variance of the free energy changes calculated from different sections of the overall trajectory of 0.2 ns length.

Using this full FEP approach, we had to take a running average of data from simulations at different heights to give the PMF for the central position, as the numerical differentiation of the PMF is very sensitive to noise. Here, we modify our approach and use FEP to directly calculate the numerical derivative of the free energy change with respect to the tip position. This derivative is then integrated numerically to obtain full free energy curves. This two step approach allows us to choose the size of the applied perturbation independently of the distance between simulation images, in principle allowing significantly larger distances between images to be used.

2.4. Simulation Setup. **2.4.1. Umbrella Sampling—Calcite.** The calcite system, depicted in Figure 2c consisted of a rectangular simulation box of approximately $4 \times 4 \times 12\text{ nm}^3$, containing seven layers of calcite, exposing the $(10\bar{1}4)$ surface perpendicular to the z direction, and 5156 water molecules. The solid–liquid interfaces consisted of 5×8 surface unit cells, each containing two Ca^{2+} and CO_3^{2-} ions. Initial simulations confirmed that the separation between periodic images of the slab was large enough to allow the water in between to reach bulk-like structure. The tip was modeled by a 125 atom (25 functional units) calcite nanocluster, which was cut from bulk then annealed in a vacuum and finally equilibrated in water. A recent study of calcite nanocluster stability³³ had found nanoparticles of either 24 or 32 functional units to be the most stable, but we deliberately chose a nonideal cluster, as this would be a more realistic model for an AFM tip termination, while still stable on the time scale of simulation. The nanocluster was oriented with its elongated axis perpendicular to the interface, to simulate a sharp tip, most likely to yield high contrast in the experiment.

We used a recently developed force field describing atomic interactions,³⁴ which uses the flexible SPC/Fw model for water and flexible carbonate ions. Molecular dynamics (MD) simulations were carried out using the GROMACS simulation suite.³⁵ Lennard-Jones and Buckingham interaction potentials were tabulated; electrostatic interactions were calculated with the particle-mesh Ewald scheme. The cutoff distance for the nonbonded interactions and the real space part of the electrostatic interaction was set to 1.1 nm. The equations of motion were integrated with the leapfrog algorithm using a time step of 1 fs. Initial velocities were drawn from a Boltzmann distribution, and a Nosé-Hoover thermostat with a time constant of $\tau_T = 0.5$ ps was used to sample a canonical ensemble at temperature $T = 300$ K. The weighted histogram analysis method (WHAM) implemented in the GROMACS distribution³⁶ was used to compute the free energy profiles from configurations saved every picosecond.

The starting configurations for the individual umbrella simulations were prepared by placing the nanocluster at different positions over the surface and adding the maximum number of water molecules (at bulk density), compatible with all nanocluster positions, to keep the number of water molecules constant in every simulation. The distances between the lowest atom in the tip and the plane of calcium atoms in the surface varied from 0.4 to 2.2 nm. The distance was incremented in steps of 0.05 nm between 0.4 and 0.8 nm, and in steps of 0.1 nm between 0.8 and 2.2 nm. This was done for 8×4 lateral positions over a surface unit cell. Each of the 736 simulations was run for 5 ns, the first 0.5 ns of which were discarded as equilibration. Calcium and carbon atoms in the nanocluster were restrained laterally by a harmonic potential with a force constant $k = 1000\text{ kJ mol}^{-1}\text{ nm}^{-2}$. Calcium and carbon atoms in the middle layer of the surface slab were constrained in x , y , and z , by a harmonic potential of the same strength, to immobilize the slab with respect to the simulation box. The force constants of the harmonic umbrella potential constraining the distance between the centers of mass of the tip and the surface slab were $10\,000\text{ kJ mol}^{-1}\text{ nm}^{-2}$ for z between 0.4 and 0.6 nm, $5000\text{ kJ mol}^{-1}\text{ nm}^{-2}$ for z between 0.7 and 1.2 nm and $1000\text{ kJ mol}^{-1}\text{ nm}^{-2}$ for z between 1.3 and 2.2 nm.

2.4.2. Umbrella Sampling—Calcium Fluoride. The simulated system is similar to our previous studies:^{26,27} the rhombohedral simulation box, measuring approximately $3.0 \times 2.6 \times 7.3\text{ nm}^3$, contained a slab of three layers of fluorite, exposing the (111) surface, perpendicular to the z direction. The construction of starting configurations and simulation setup is similar to the calcite system, unless otherwise specified. The 72 atom fluorite nanocluster, representing the AFM tip, was oriented in such a way that a sharp, fluorine terminated end pointed toward the surface. The umbrella potential acted on the z coordinate of the distance vector between the center of mass of the surface slab and the center of mass of either the entire tip or the upper 48 atoms in the tip. The lateral tip position was restrained independently, by a harmonic potential acting in x and y , either on all tip atoms or the upper 48 atoms only. The system is depicted in Figure 2b.

Calcium fluoride and water interaction parameters were taken from de Leeuw and Cooper,³⁷ discarding the polarizability terms, and the TIP4P/2005 potential was used to model water, as in our previous studies.^{26,27} The cutoff distance for the nonbonded interactions and the real space part of the electrostatic interaction was set to 0.9 nm. The equations of motion were integrated with the leapfrog algorithm using a

time step of 2 fs. Initial velocities were drawn from a Boltzmann distribution, and a Nosé-Hoover thermostat with a time constant of $\tau_T = 1$ ps was used to sample a canonical ensemble at temperature $T = 300$ K. We used the LINCS algorithm to keep the water molecule geometry rigid. The weighted histogram analysis method (WHAM) implemented in the GROMACS distribution³⁶ was used to compute the free energy profiles and an error estimate.

Free energy calculations were performed for tip approaches over calcium (Ca), protruding fluorine (Fh), and subsurface fluorine (Fl) atomic sites in the surface (see Figure 1). Starting configurations were set up with the distance between the surface and the lowest atom in the tip ranging from 0.2 to 1.2 nm. Between 0.2 and 0.5 nm, the tip–surface distance was incremented in steps of 0.05 nm, and the harmonic umbrella potential had a force constant $k = 20\,000$ kJ mol⁻¹ nm⁻². Between 0.50 and 1.20 nm, increments of 0.1 nm were used, and the force constant was reduced to $k = 10\,000$ kJ mol⁻¹ nm⁻². Each MD trajectory was run for 5 ns, the first 0.5 ns of which were discarded as equilibration. After an initial umbrella sampling run, for the free energy calculation over Ca, additional windows at a 0.275, 0.325, and 0.375 nm tip–surface distance were simulated, with an umbrella potential force constant of $k = 40\,000$ kJ mol⁻¹ nm⁻², to obtain a satisfying overlap of $P(z)$ between neighboring windows.

We point out that the different values of umbrella potential force constants in calcite and fluorite were chosen empirically, to obtain sufficient overlap of distributions in neighboring windows, in a fixed amount of computation time. They are not a quantitative measure of tip–surface interaction strengths at certain distances, as can be seen from the variations in the resulting free energy profiles.

2.4.3. Free Energy Perturbation Calculations. The setups of the systems in terms of numbers of atoms etc. were identical to those detailed above for the umbrella sampling calculations.

The fluorite system is identical to our previous studies.^{26,27} The upper half of the tip was frozen, and images were separated by 0.01 nm. We investigated the effect of using different perturbation step sizes on the calculated PMFs. For this system, an NpT ensemble was used to sample configurations.

For studies on calcite, we carried out calculations in an NVT ensemble. The entire tip was fixed and unable to relax. The images were separated by 0.015 nm, and a perturbation size of 0.001 nm was used.

3. RESULTS

3.1. Calcium Fluoride. In Figure 4, we present free energy profiles obtained over the calcium and two fluorine surface sites of the fluorite (111) surface using the two calculation approaches.

The free energy profiles obtained with umbrella sampling and free energy perturbation are in near quantitative agreement. Both methods are equally suited for further comparison with experimental data, through force–distance curves derived from free energy profiles, or simulated AFM images. This demonstrates one of our aims. We find that the umbrella sampling method is somewhat more efficient than our original FEP calculations.

The calculations show significant differences in the free energy for the approach over different surface sites, with variations in energy of similar magnitude to those observed in a vacuum and shown to provide good atomic contrast. Converting the PMF into force curves experienced by the tip

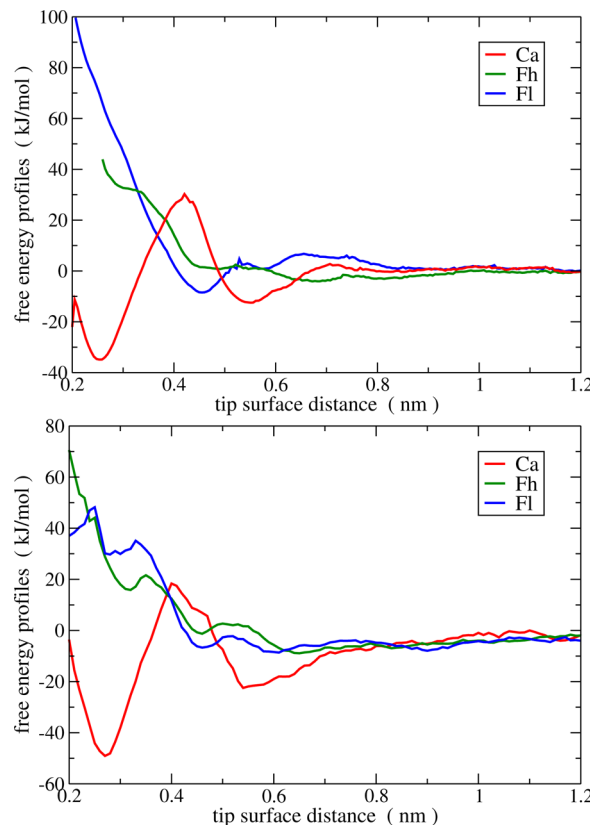


Figure 4. Free energy profiles over calcium (Ca), protruding fluorine (Fh), and subsurface fluorine (Fl) in CaF_2 obtained with umbrella sampling in the NVT ensemble (top) and with FEP/thermodynamic integration in the NpT ensemble (bottom).

on approaching the surface, we find that between differing surface locations there is a statistically significant contrast in the force exerted upon the tip. The converged calculations clearly show that there is a region from 0.25 to 0.6 nm where distinct contrast between sites can be observed.

We decomposed the free energy calculated using the FEP in various ways: into potential energy and entropic contributions and into terms arising from the direct interaction of the tip and surface and those mediated by the solvating water. We have also considered the same tip approach in a vacuum. The decomposition showed that the total free energy change is a small difference between large potential energy and entropic terms. The entropic term is mostly attractive and principally consists of the increase in translational and rotational degrees of freedom when water initially confined near the tip or surface is forced away into bulk like positions, due to tip–surface proximity. That this is the case is clearly illustrated by comparison to calculations in a vacuum, where the evolution of potential energy is almost indistinguishable from the overall free energy change and is consistent with the use of static calculations to understand nc-AFM measurements in UHV.

Decomposition into energy change due to direct interaction of the tip and surface and the energy change mediated by the solvent showed that above the Ca^{2+} cation site this system has a rather strong direct tip–surface interaction that partially controls the appearance of a free energy well at around 0.2 nm. However, as the direct interaction is now only a component of the total system energy, the direct tip–surface interaction is smaller than that in a vacuum, and at larger

distances and above anions indirect interactions due to water reconstructing are dominant.

3.1.1. Perturbation Size in FEP. In trying to optimize this method for computational efficiency and numerical accuracy/stability, we attempted to increase the size of the perturbations, allowing images to be more widely spaced, particularly when the tip was far from the surface, as used in the umbrella sampling calculations. However, we found that our original perturbation of ± 0.005 nm was at the limit of perturbation step-size that is numerically stable for our system. A perturbation of ± 0.001 nm results in much less noise in the calculated PMF, as shown in Figure 5. We note that the perturbation size in our simulations is a numerical parameter, not related to the cantilever oscillation amplitude, or other parameters in FM-AFM experiments.

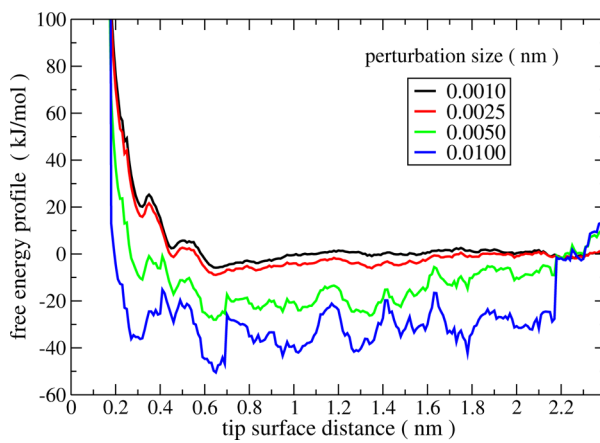


Figure 5. Free energy profiles over protruding fluorine (Fh) with FEP/thermodynamic integration in the (NpT) ensemble with varying sizes of the perturbation applied to the tip (in nm).

In fact, the main observable of interest for nc-AFM simulation is the derivative of the free energy with respect to tip height rather than dG itself. This can be numerically found rather stably from small perturbations toward and away from the surface. The total PMF can then be reconstructed by numerical integration, if required. Still we find that the data points must be closely spaced to obtain smooth curves, and we are limited by the curvature of the PMF in the regions of main interest to around a 0.02 nm spacing. Even optimizing as best as we can, the FEP is several times more costly than the umbrella sampling method.

As we have shown that we can obtain quantitative agreement between the two methods, we have focused on the more efficient umbrella sampling technique to explore the other technical parameters that need to be controlled. In the next section, we show that we can produce robust results on the more complex calcite system using this approach. We also examine the boundary conditions applied to the umbrella sampling calculations to keep the tip in place and show that they are sufficient to cover the remaining small differences between the FEP and umbrella sampling calculations.

3.2. Calcite. **3.2.1. Hydration Layer Structure.** In order to study the hydration layer structures over the calcite ($10\bar{1}4$) surface, we simulated a system consisting only of a calcite surface slab and water, without a nanocluster tip. We averaged atomic positions over 3 ns of MD in the NpT ensemble. The observed hydration layer structures are presented in Figure 6.

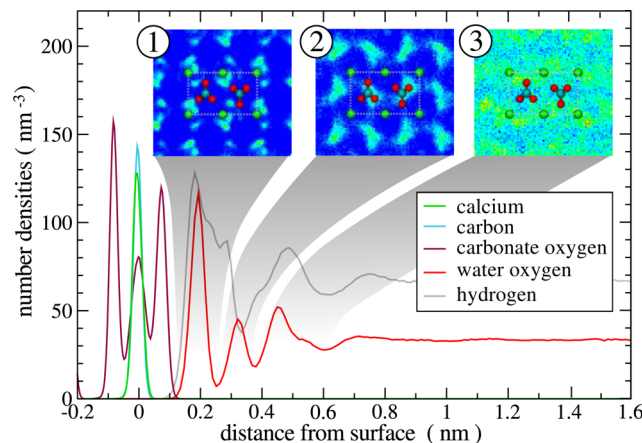


Figure 6. Hydration layer structure over calcite ($10\bar{1}4$) from simulation: density profiles along z , perpendicular to the surface, indicate there are three distinct hydration layers over the surface. Small insets show water molecule oxygen density maps in (x,y)-planes within the hydration layers, and the surface unit cell underneath.

The hydration layer structures over calcite and fluorite share some similarities: water molecules in the first hydration layer are situated above surface calcium ions, water molecules in the second layer are situated over the protruding negatively charged ion. The position of third layer water molecules is different: in fluorite, these are situated over the subsurface fluoride ion, whereas in calcite they are located over calcium ions, although the lateral ordering in the third layer is quite weak for both systems.

We note that the hydration layer structures we obtained, using the newer, flexible set of potentials,³⁴ differ slightly from the ones obtained with the original set of potentials by the same authors.³⁸ The peaks in the water oxygen density are at the same distances from the surface, but the height of the second peak is lower when using the newer force field. Also, the water molecule oxygen atom positions with respect to the surface atoms are similar in the first and second layers but differ in the third layer.

The two force fields use different potentials for water. In the original version, intramolecular bonds and angles in water and carbonate ions are rigid, and the TIP4P-Ew potential³⁹ is used for water. In the newer, flexible version, harmonic terms for bonds and angles are added to the potential, and the SPC/Fw potential⁴⁰ is used instead of TIP4P. The authors have refitted the calcite–water interaction parameters to reproduce the correct free energies of solvation. Nevertheless, the magnitudes and positions of the point charges on the SPC/Fw water molecule are different from the ones on TIP4P-Ew, and this is responsible for the small discrepancies in the hydration layer structures observed in the simulations. Without a direct comparison to experimental force spectroscopy, we cannot at this point comment on the accuracy of either model.⁴¹

3.2.2. Free Energy Profiles from Umbrella Sampling. In Figure 7, we present four of a total of 32 free energy profiles obtained over one calcite surface unit cell, corresponding to tip approaches over the two calcium and carbonate ions. The calcite nanocluster tip was effectively terminated by a negatively charged carbonate group, with a high rotational mobility. The free energy profiles are flat at large tip–surface separations ($z \geq 1.2$ nm). As the tip approaches the surface ($0.8 \text{ nm} \leq z \leq 1.2 \text{ nm}$), small free energy barriers appear, due to the interactions between hydration layers over the surface and water molecules

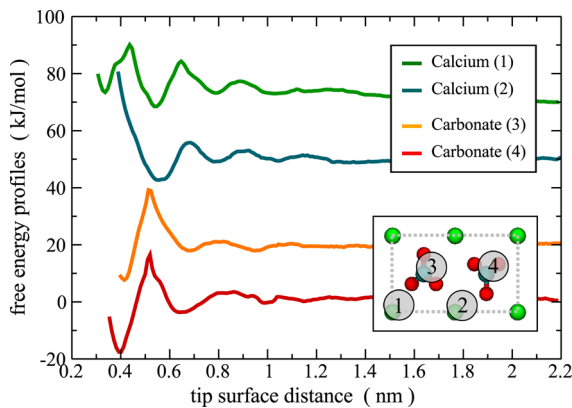


Figure 7. Free energy profiles over the two calcium and carbonate groups in a calcite surface unit cell, obtained with umbrella sampling in the NVT ensemble.

solvating the tip. For the tip approach over calcium, the tip apex starts to interact directly with the third hydration layer at $0.6 \text{ nm} \leq z \leq 0.8 \text{ nm}$. The increase in free energy for $z \leq 0.6 \text{ nm}$ is due to the interaction with the first hydration layer. The subsequent drop in free energy observed in the first profile for $z \leq 0.45 \text{ nm}$ corresponds to a jump-to-contact of the mobile carbonate group at the tip apex. For the tip approach over carbonate groups, we observe a free energy barrier at $0.4 \text{ nm} \leq z \leq 0.7 \text{ nm}$, caused by the interaction with water molecules in the second hydration layer.

We conclude that the differences between the free energy profiles over calcium and carbonate ions obtained from our simulations are in agreement with the capability to achieve atomic resolution in experimental AFM images of this surface in water.⁸ A more quantitative analysis of the free energy profiles in terms of perturbations of hydration layer structures as well as simulated AFM images based on the force–distance maps derived from these free energy profiles will be published elsewhere along with detailed experimental results.⁴¹

3.2.3. Free Energy Profiles from FEP. We also attempted to carry out FEP calculations for the approach of the tip over representative cation and anion sites on the calcite surface. We found that the FEP calculations were hard to converge for the calcite system. In Figure 8, we show free energy profiles obtained with a completely frozen tip. These data were

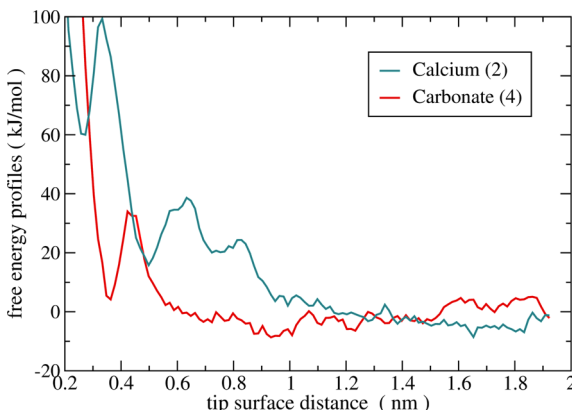


Figure 8. Free energy profiles over calcium and carbonate ions in a calcite surface unit cell, obtained with FEP in the NVT ensemble, using a frozen tip. To be compared with second and fourth energy profiles in Figure 7.

collected for 9 ns with trajectories sampled every 5 ps. We get good qualitative agreement with the umbrella sampling: The free energies are significantly higher than for the umbrella sampling calculation with a partially mobile tip, but the positions of the free energy extrema are in very good agreement. Larger free energies are expected as the tip is unable to relax to accommodate the interaction with the surface. These calculations do indicate that the ability of the tip to relax is not a dominant contributor to the force contrast at different sites. Additional 5 ns simulations allowing the lower third of the tip to relax did not produce reasonably well converged free energy curves.

4. ACCURACY

Since we are forced to model the AFM tip as a nanocluster, we need to constrain lateral translational and rotational degrees of freedom in a systematic way, to account for the missing macroscopic part of the tip and cantilever. This will have an influence on other degrees of freedom of the system as well and will affect the free energy profile obtained. In order to measure this effect, we have performed umbrella sampling simulations on the fluorite system, varying the way in which the lateral constraint to the tip and the umbrella potential were applied. We also compared umbrella sampling in the NVT and *NpT* ensembles. Finally, we have studied the convergence of the collective variable histograms in the umbrella windows.

4.1. Tip Constraints. We calculated the free energy in NVT for tip approaches over a surface calcium site, with different constraints on the tip: the umbrella potential and the lateral harmonic restraints could act either on all atoms in the tip or only on the upper 48 atoms. The center of mass of the surface slab was always taken as the other reference point for the umbrella potential. The results shown in Figure 9 indicate that

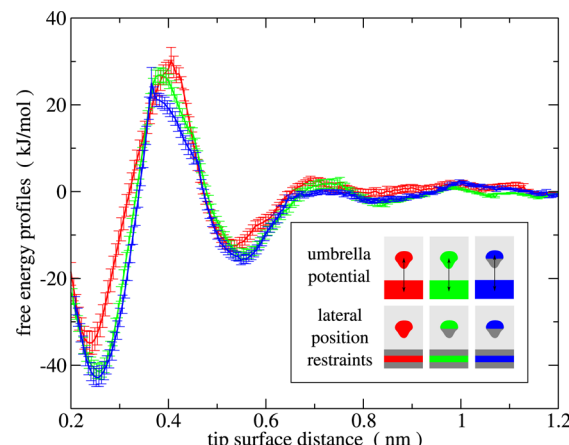


Figure 9. Influence of lateral tip position constraints and umbrella potential on the free energy profile over calcium in CaF_2 . In the legend, the constrained parts of the system are highlighted in color, whereas the unconstrained parts of tip and surface are dark gray, and the liquid is light gray.

the general shape of the free energy profile is not affected by the choice of constraints. As expected, free energy values become slightly lower as the number of constrained degrees of freedom is reduced, but the changes are on the same order of magnitude as the statistical errors of the WHAM calculation.

4.2. *NpT* vs *NVT* Ensemble. We also calculated the free energy profile for a tip approach over a surface calcium site in

the isothermal–isobaric ensemble. We took the same initial configurations as for the *NVT* umbrella windows but applied a semi-isotropic Parrinello–Rahman barostat with a time constant $\tau_p = 10$ ps to maintain a pressure of $p = 1$ bar. The trajectory length was increased to 7 ns, and the first 2 ns were discarded as equilibration. The protocol for the umbrella potentials and the lateral tip constraints was identical to the *NVT* simulation. The free energy profiles obtained in both ensembles, $\Delta G(z)$ and $\Delta F(z)$, are shown in Figure 10. Although the absolute differences are as large as 10 kJ mol⁻¹, the shapes of the profiles are very similar.

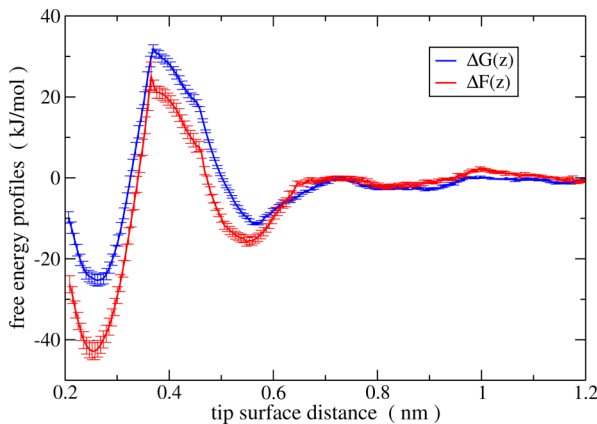


Figure 10. Comparison of free energy profiles over calcium in CaF_2 , obtained from constant pressure (ΔG) and constant volume (ΔF) simulations.

We note that this type of mixed system, consisting of a solid and a liquid, with periodic boundaries is not well suited for *NpT* simulations: the main purpose of the barostat is to ensure that the solvent reaches bulk density away from the surfaces. But since the pressure is calculated from the virial, very small changes in the length of the box vectors parallel to the solid slab will lead to huge changes in pressure and oscillations of the box vectors. In our simulation, we fixed the box vectors in x and y according to the equilibrium values of the fluorite unit cell vectors and effectively only allowed the box vector in z to fluctuate. This still leads to box vector oscillations in z but yields a more accurate behavior of the system.

4.3. Convergence of Umbrella Sampling Histograms.

The accuracy of the free energy profile calculated with umbrella sampling depends on the following: (i) the collective variable histograms of neighboring umbrella windows need to overlap and (ii) the histograms in each window need to be converged.

In Figure 11, we present the time evolution of histograms of the tip–surface distance obtained for a tip approach over a calcium atom in CaF_2 , in the *NpT* ensemble simulation. The total simulation time was 7 ns, and the first nanosecond was discarded as equilibration time. For this particular system, it takes at least 5 ns of time averaging to converge the histograms. We also note that there is only a small overlap between windows numbered 6 and 7, as well as 8 and 9, which limits the accuracy of the corresponding free energy profile shown in Figure 10. To improve accuracy, two additional windows, with a stronger umbrella potential, could be introduced to cover the regions of z that are poorly sampled. Also, the simulation time in each window could be increased even further.

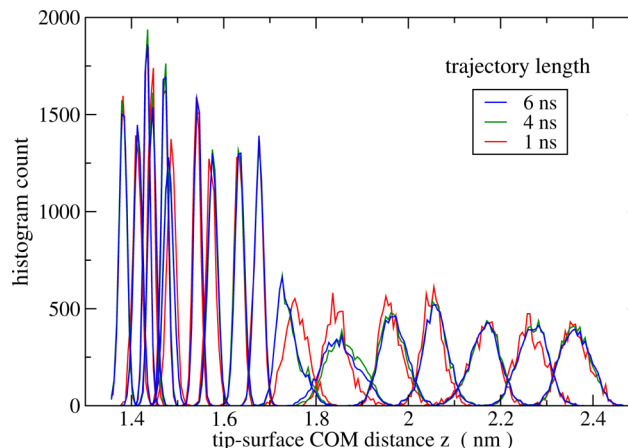


Figure 11. Convergence of the histograms of the collective variable z in umbrella sampling windows, for a tip approach over a calcium ion in the CaF_2 surface. The histograms were obtained after 1 (red), 4 (green), and 6 ns (blue) of MD sampling in *NpT*.

5. DISCUSSION

The free energy profiles obtained with umbrella sampling and free energy perturbation are in quantitative agreement. Both methods are equally suited for further comparison with experimental data, through force–distance curves derived from free energy profiles, or simulated AFM images. This also suggests that the different methods of constraining the tip to a fixed orientation with respect to the surface are essentially equivalent for our purposes, though we investigated this boundary condition more carefully with the more efficient umbrella sampling method.

The free energy calculation based on umbrella sampling is robust with respect to the application of the umbrella potential, as well as the lateral constraints of the tip. As long as the constant volume simulations are carried out with the correct solvent density in the bulk-like region of the system, they yield similar free energies to those of the constant pressure simulations. To this end, the simulation box size should be equilibrated in *NpT* first, before individual umbrella windows are run in *NVT* MD. A drawback of the umbrella sampling simulation protocol is the lack of an *a priori* optimum choice for the spacing of umbrella windows, and strength of umbrella potentials, to obtain a good overlap of the distribution of the collective variable, $P(z)$, in neighboring windows. It may be necessary to run additional windows and/or increase the strength of the umbrella potential in subsequent simulations.

We have optimized the protocols for carrying out FEP simulations of this system, offering a big speed up over our original calculations and improving the accuracy of the constructed free energy surfaces. But, the FEP method is still several times more costly than umbrella sampling. However, an advantage of the FEP is the ability to decompose the free energy changes into components within a single simulation.¹⁹ Two distinct decompositions of the free energy seem to be beneficial in understanding AFM contrast mechanisms:

(i) The direct interaction between tip and surface can be found by repeating the perturbation procedure, on the same ensemble sampled from the full trajectory, but setting the charge, and any nonbonding interactions involving constituents of water molecules, to zero. The difference between this direct contribution and the total free energy change then comes from water mediated interactions. The direct interaction is different

from the vacuum interaction because the configurations to which the perturbations are applied come from a molecular dynamics trajectory evolved under the influence of the full Hamiltonian.

(ii) A break down into entropic and potential components by subtracting the potential energy from the free energy (both terms are directly evaluated during the PMF calculation) is performed to identify the entropic contribution to the free energy change.

The decomposition into direct and water mediated interactions is robust and readily achieved through post processing saved trajectories. However, converging the potential energy sufficiently to obtain a good decomposition into entropic and enthalpic contributions can be challenging and expensive. A further caveat is whether the force field employed is expected to give a good representation of the individual components of the free energy—or just the total free energy at the given temperature at which the force field was trained. Nonetheless, these analysis tools are useful in understanding the mechanisms of imaging in solution.

In summary, we have shown that both free energy approaches discussed are capable of statistically accurate calculations of short-range tip–surface interaction forces. Direct comparison between the methods yields near quantitative agreement, despite being based on rather different theoretical approaches. For the calcite system, it proves extremely difficult to converge the FEP calculations, and we demonstrate that the umbrella sampling method is more efficient in general for *soft* systems. However the FEP method does offer advantages in data analysis, which is particularly useful when analyzing the interaction components in real experiments. Certainly, having access to both tools for any given system is likely to greatly increase the impact of any simulations and improve the reliability of the comparison to experiment.

We hope that these results will encourage workers in solid/liquid interfaces to consider recent developments in AFM technology as both a tool for probing water structure in 3D but also a playground for exploring, and improving, free energy methods.

AUTHOR INFORMATION

Corresponding Author

*E-mail: bernhard.reischl@tut.fi

Notes

The authors declare no competing financial interest.

ACKNOWLEDGMENTS

This research has been supported by the Academy of Finland through its Centres of Excellence Program (project no. 251748). B.R. is supported by the Finnish Cultural Foundation through a 3 year doctoral study grant. M.W. is supported by the Leverhulme Trust (grant F/07 134/CK) and acknowledges the HPC-EUROPA2 project for funding visits to Finland under the Transnational Access Programme. We acknowledge very useful discussions and comments on the manuscript from Alexander Shluger.

REFERENCES

- (1) Müller, D. J.; Dufrêne, Y. F. *Nat. Nanotechnol.* **2008**, *3*, 261–269.
- (2) Rounsevell, R. *Methods* **2004**, *34*, 100–111.
- (3) Shakhnovich, E. *Chem. Rev.* **2006**, *106*, 1559–1588.
- (4) Barth, C.; Foster, A. S.; Henry, C. R.; Shluger, A. L. *Adv. Mater.* **2011**, *23*, 477–501.
- (5) Giessibl, F. *Rev. Mod. Phys.* **2003**, *75*, 949–983.
- (6) Fukuma, T.; Kobayashi, K.; Matsushige, K.; Yamada, H. *Appl. Phys. Lett.* **2005**, *87*, 034101.
- (7) Fukuma, T.; Higgins, M.; Jarvis, S. *Phys. Rev. Lett.* **2007**, *98*, 106101.
- (8) Rode, S.; Oyabu, N.; Kobayashi, K.; Yamada, H.; Kühnle, A. *Langmuir* **2009**, *25*, 2850–2853.
- (9) Hiasa, T.; Kimura, K.; Onishi, H.; Ohta, M.; Watanabe, K.; Kokawa, R.; Oyabu, N.; Kobayashi, K.; Yamada, H. *J. Phys. Chem. C* **2010**, *114*, 21423–21426.
- (10) Fukuma, T.; Ueda, Y.; Yoshioka, S.; Asakawa, H. *Phys. Rev. Lett.* **2010**, *104*, 016101.
- (11) Hiasa, T.; Kimura, K.; Onishi, H. *Phys. Chem. Chem. Phys.* **2012**, *14*, 8419–8424.
- (12) Sader, J. E.; Jarvis, S. P. *Appl. Phys. Lett.* **2004**, *84*, 1801.
- (13) Schneeweiss, P.; Gierling, M.; Visanescu, G.; Kern, D.; Judd, T.; Günther, A.; Fortagh, J. *Nat. Nanotechnol.* **2012**, *7*, 515–519.
- (14) Wong-Ekkabut, J.; Baoukina, S.; Triampo, W.; Tang, I.-M.; Tieleman, D. P.; Monticelli, L. *Nat. Nanotechnol.* **2008**, *3*, 363–368.
- (15) Lin, J.; Zhang, H.; Chen, Z.; Zheng, Y. *ACS Nano* **2010**, *4*, 5421–5429.
- (16) López, C. A.; de Vries, A. H.; Marrink, S. J. *PLoS Comput. Biol.* **2011**, *7*, e1002020.
- (17) Patel, A. J.; Varilly, P.; Jamadagni, S. N.; Hagan, M. F.; Chandler, D.; Garde, S. *J. Phys. Chem. B* **2012**, *116*, 2498–2503.
- (18) Li, T.; Gao, J.; Szoszkiewicz, R.; Landman, U.; Riedo, E. *Phys. Rev. B* **2007**, *75*, 115415.
- (19) Eun, C.; Berkowitz, M. *J. Phys. Chem. B* **2009**, *113*, 13222–13228.
- (20) Labuda, A.; Paul, W.; Pietrobon, B.; Lennox, R.; Grütter, P.; Bennewitz, R. *Rev. Sci. Instrum.* **2010**, *81*, 083701.
- (21) Kantorovich, L.; Trevethan, T. *Phys. Rev. Lett.* **2004**, *93*, 236102.
- (22) Federici Canova, F.; Foster, A. S. *Nanotechnology* **2011**, *22*, 045702.
- (23) Kawai, S.; Canova, F. F.; Glatzel, T.; Foster, A. S.; Meyer, E. *Phys. Rev. B* **2011**, *84*, 115415.
- (24) Schütte, J.; Rahe, P.; Tröger, L.; Rode, S.; Bechstein, R.; Reichling, M.; Kühnle, A. *Langmuir* **2010**, *26*, 8295–8300.
- (25) Barth, C.; Foster, A.; Reichling, M.; Shluger, A. *J. Phys.: Condens. Matter* **2001**, *13*, 2061–2079.
- (26) Watkins, M.; Shluger, A. L. *Phys. Rev. Lett.* **2010**, *105*, 196101.
- (27) Watkins, M.; Berkowitz, M. L.; Shluger, A. L. *Phys. Chem. Chem. Phys.* **2011**, *13*, 12584–12594.
- (28) Fukuma, T. Private communication.
- (29) Torrie, G. M.; Valleau, J. P. *Chem. Phys. Lett.* **1974**, *28*, 578–581.
- (30) Kumar, S.; Bouzida, D.; Swendsen, R. H.; Kollman, P. A.; Rosenberg, J. M. *J. Comput. Chem.* **1992**, *13*, 1011–1021.
- (31) Zwanzig, R. W. *J. Chem. Phys.* **1954**, *22*, 1420–1426.
- (32) Choudhury, N.; Pettitt, B. M. *J. Am. Chem. Soc.* **2005**, *127*, 3556–3567.
- (33) Cooke, D. J.; Elliott, J. A. *J. Chem. Phys.* **2007**, *127*, 104706.
- (34) Raiteri, P.; Gale, J. D. *J. Am. Chem. Soc.* **2010**, *132*, 17623–17634.
- (35) Hess, B.; Kutzner, C.; van der Spoel, D.; Lindahl, E. *J. Chem. Theory Comput.* **2008**, *4*, 435–447.
- (36) Hub, J. S.; de Groot, B. L.; van der Spoel, D. *J. Chem. Theory Comput.* **2010**, *6*, 3713–3720.
- (37) de Leeuw, N. H.; Cooper, T. G. *J. Mater. Chem.* **2002**, *13*, 93–101.
- (38) Raiteri, P.; Gale, J. D.; Quigley, D.; Rodger, P. M. *J. Phys. Chem. C* **2010**, *114*, 5997–6010.
- (39) Horn, H. W.; Swope, W. C.; Pitera, J. W.; Madura, J. D.; Dick, T. J.; Hura, G. L.; Head-Gordon, T. *J. Chem. Phys.* **2004**, *120*, 9665–9679.
- (40) Wu, Y.; Tepper, H. L.; Voth, G. A. *J. Chem. Phys.* **2006**, *124*, 024503.
- (41) Reischl, B.; Federici, F.; Foster, A. S.; Kobayashi, N.; Fukuma, T. In preparation.